

## On the spatial structure of coastal circulation off Newport, Oregon, during spring and summer 2001 in a region of varying shelf width

P. Michael Kosro

College of Oceanic and Atmospheric Sciences, Oregon State University, Corvallis, Oregon, USA

Received 15 October 2004; revised 3 August 2005; accepted 23 August 2005; published 29 October 2005.

[1] A time series of hourly surface current maps in the shelf waters off Newport, Oregon, was made during April–September 2001 using five SeaSonde HF current mappers, during Coastal Advances in Shelf Transport (COAST). The surface currents responded rapidly to the changing winds, in repeated patterns that were strongly affected by bottom topography. An equatorward current jet repeatedly formed in response to upwelling winds, its strength, but not its trajectory, covarying with the meridional wind stress. Near Cape Foulweather (44.8°N), where the shelf begins to widen, the jet rotates, weakens, and trends offshore to the south first along, then across, the isobaths. Below Cape Foulweather, inshore of the jet, a lee region of generally weak currents was commonly observed. The equatorward jet core was most commonly observed near the 80-m isobath between 45.0°N and 44.4°N, but transited offshore between spring and summer over Heceta Bank. At Newport (44.6°N), it was rarely observed less than 8 km from the coast. A second, inshore, equatorward jet, previously unknown, was observed repeatedly south of Waldport (44.4°N). Sustained downwelling wind episodes produced poleward currents, though less responsively north of Cape Foulweather. Strongest poleward flow was generally trapped near the coast. Surface currents were correlated with the northward wind, except regionally far from shore over Heceta Bank, responding within half a day. Response to the wind varies spatially, being intensified in the narrow shelf (northern) region. The equatorward jet persists through periods of zero wind forcing. Coastal sea level covaries with the meridional wind and the primary mode of ocean current response.

**Citation:** Kosro, P. M. (2005), On the spatial structure of coastal circulation off Newport, Oregon, during spring and summer 2001 in a region of varying shelf width, *J. Geophys. Res.*, 110, C10S06, doi:10.1029/2004JC002769.

### 1. Background

[2] Coastal upwelling circulation off Oregon has been examined in a series of coordinated field and modeling studies, beginning with the Coastal Upwelling Experiment in 1972 (CUE-1) and 1973 (CUE-2) [Richards, 1981]. In response to equatorward winds during the spring and summer, an upwelling cross-shore circulation raises density surfaces and lowers sea level toward coast. The resulting cross-shore pressure gradient force is largely geostrophically balanced by a surface-intensified equatorward current jet [Allen, 1973; Huyer *et al.*, 1975; Jones and Halpern, 1981]. These responses tend to persist following a seasonal triggering event, the spring transition [Huyer *et al.*, 1979; Strub *et al.*, 1987]. Analysis of moored current measurements indicate that the vertically averaged currents during the upwelling season tend to align with the local bottom topography [Kundu and Allen, 1976]. Although the coastal jet is expected to be aligned largely alongshore, the departure of the coastal jet from the shelf and upper slope out to the deep ocean was observed off northern California during the CODE experiment [Davis, 1985; Kosro, 1987; Kosro

and Huyer, 1986], and episodic separation of the coastal jet from the southern Oregon shelf near Cape Blanco has been established [Barth *et al.*, 2000; Barth and Smith, 1998]. The high cross-shelf transport represented by separation of the coastal jet indicates that it has the potential to be an important contributor to cross-shelf exchange.

[3] In this study, the mean and time-varying elements of the surface circulation are examined off the central Oregon coast, in a region of complex bathymetry (the shelf width increases by a factor of five in 150 km alongshore, and submarine banks are present over the shelf). Here coastal currents can vary strongly across shore (e.g., across the coastal jet), alongshore (e.g., owing to varying shelf width) and in time (e.g., owing to wind forcing), so that it is important to resolve the coastal flow synoptically and repeatedly. For this study, an array of HF surface current mappers [Barrick *et al.*, 1977] has been used to obtain a 6-month time series of surface current maps during the upwelling season of 2001, with resolution of 1 hour in time, 2 km in range, and 5 degrees in azimuth, over a region 100 km alongshore and up to 40 km across shore, in a region of varied bathymetry. With these measurements, an overview is sought of the spatially varying components of the coastal surface circulation, including the equatorward current jets, the poleward nearshore jet, and the lee region of

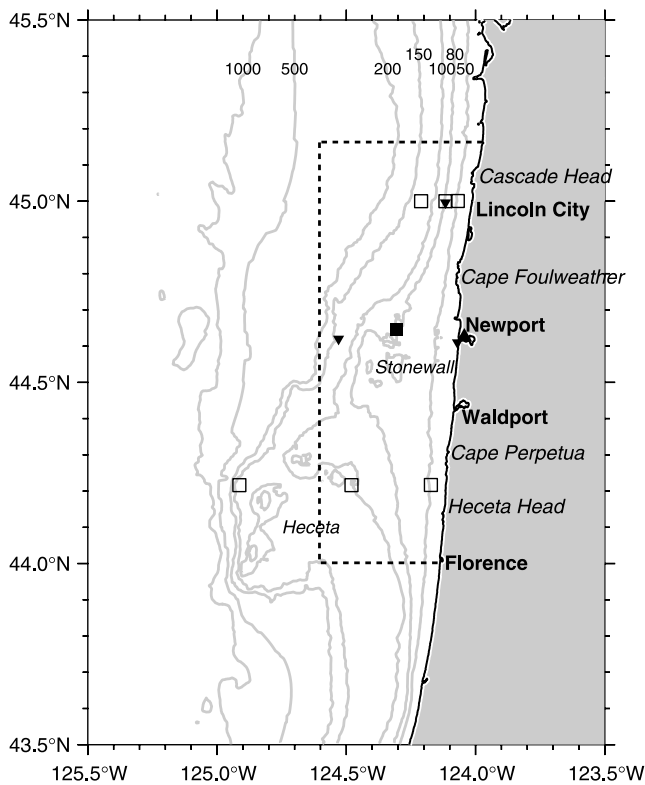


**Figure 1.** Coastal bathymetry off Newport, Oregon, is dominated by a large bank complex which includes Stonewall and Heceta banks. Time series data from moorings (boxes), meteorological sensors (downward triangles), and a tide-gauge (upward triangle) are available for the summer of 2001. Dashed line indicates area shown in subsequent maps of HF surface currents.

weak currents, including their time variation under wind forcing and their variation with bottom topography.

[4] In the following, we first examine the time-dependent coastal response to two sets of wind forcings: the intermittent upwelling/downwelling forcing of May 2001, and the sustained downwelling event of late August 2001. The strength and trajectory of the equatorward coastal jet, both in the mean and throughout the upwelling season, are then examined, and found to be strongly affected by shelf topography, as well as by alongshore winds; the properties of the poleward nearshore jet are also discussed. The spatial variation in the wind-correlated response of surface currents is then studied.

## 2. Measurements

[5] The Coastal Advances in Shelf Transport (COAST) experiment was designed to study the processes of cross-shore transport in regions of simple and complex topography along the Oregon shelf [Barth and Wheeler, 2005] and, in particular, to examine the behavior of cross-shelf transport by the alongshore coastal jet. The COAST experiment took place off the central Oregon coast (Figure 1). The coastline in this region is generally straight, tending along  $005^{\circ}\text{T}$  between  $44^{\circ}\text{N}$  and  $45^{\circ}\text{N}$ . In contrast, the shelf width varies dramatically alongshore. The 150-m isobath, found

less than 13 km offshore at  $45.2^{\circ}\text{N}$ , is 62 km offshore at  $44^{\circ}\text{N}$ : a fivefold increase in shelf width due to the presence of Stonewall Bank and Heceta Bank. Near  $43.9^{\circ}\text{N}$ , the shelf abruptly narrows again. The steepness of the upper continental slope varies in the opposite sense alongshore; the distance between the 150-m and 1000-m isobaths drops nearly tenfold, from 58 km at  $45.2^{\circ}\text{N}$  to 6 km at  $44^{\circ}\text{N}$ . We will refer to this region of widening shelf and steepening upper continental slope as the Heceta Bank complex.

[6] During the COAST experiment, an array of five SeaSonde HF surface current mappers was operated on the central Oregon coast, between Heceta Head ( $44.1^{\circ}\text{N}$ ) and Cascade Head ( $45.1^{\circ}\text{N}$ ) (Figure 2; Table 1). These systems, manufactured by CODAR Ocean Sensors, consist of a whip transmit antenna, a compact direction-finding receive antenna, electronics for broadcasting and receiving HF radio signals, and a data acquisition computer. Measurement theory for these systems has been described [Barrick et al., 1977; Lipa and Barrick, 1983]. At each 2-km-wide range ring, the Bragg peak in the spectrum of backscattered energy is examined frequency by frequency; the anomalous Doppler shift (beyond that expected for a surface wave at the Bragg wavelength in deep water, traveling in a quiescent ocean) gives the sign and size of the radial current. Direction finding, based on crossed-loop receive antennas, is used to determine the azimuth of the echo, within the range ring. The HF frequency varied by site between 12.1 and 13.5 MHz (Table 1). Raw measurements were made twice per second. Spectra were estimated every 10 min, producing intermediate radial maps. The intermediate maps were then combined into hourly radial maps, which were used for further analysis. Measured antenna response patterns [Barrick and Lipa, 1999] were substituted for ideal patterns in direction-finding for the Waldport site. Use of measured patterns was found to degrade the uniformity of spatial coverage in the measurements, and so their use was limited to Waldport, where the radial currents resulting from patterns more accurately resembled those from moored current measurements at NH-10 (P. M. Kosro, manuscript in preparation, 2005). Correlations between low-pass filtered currents at the surface from the HF and currents at 10 m, measured with an upward-looking acoustic Doppler profiler in 81 m water depth off Newport (Figure 1), were 0.80 and 0.83 for the eastward and northward components, respectively.

[7] Horizontal vector maps of surface currents were estimated for each hour on a fixed 2-km grid by combining the available radial component data within 4 km of each node, using a least squares procedure; a Matlab-based processing package developed at the Naval Postgraduate School [Cook and Paduan, 2001], based on the method of Gurgel [1994], was used for this purpose. Regions where geometric error amplification in either the eastward or northward current [Chapman et al., 1997] (see also D. Barrick, Geometric dilution of statistical accuracy in multi-static HF radar networks, 2002, available at [http://www.codaros.com/Manuals/Informative/GDOSA\\_Definition.pdf](http://www.codaros.com/Manuals/Informative/GDOSA_Definition.pdf)) exceeded a factor of 2, based on the nearest site pair, were discarded; the excluded regions either lie near the baseline, far from the coast, or significantly beyond the array to the north or south. This data set is used for further analysis in this paper. Surface current vectors were also estimated in near real time,

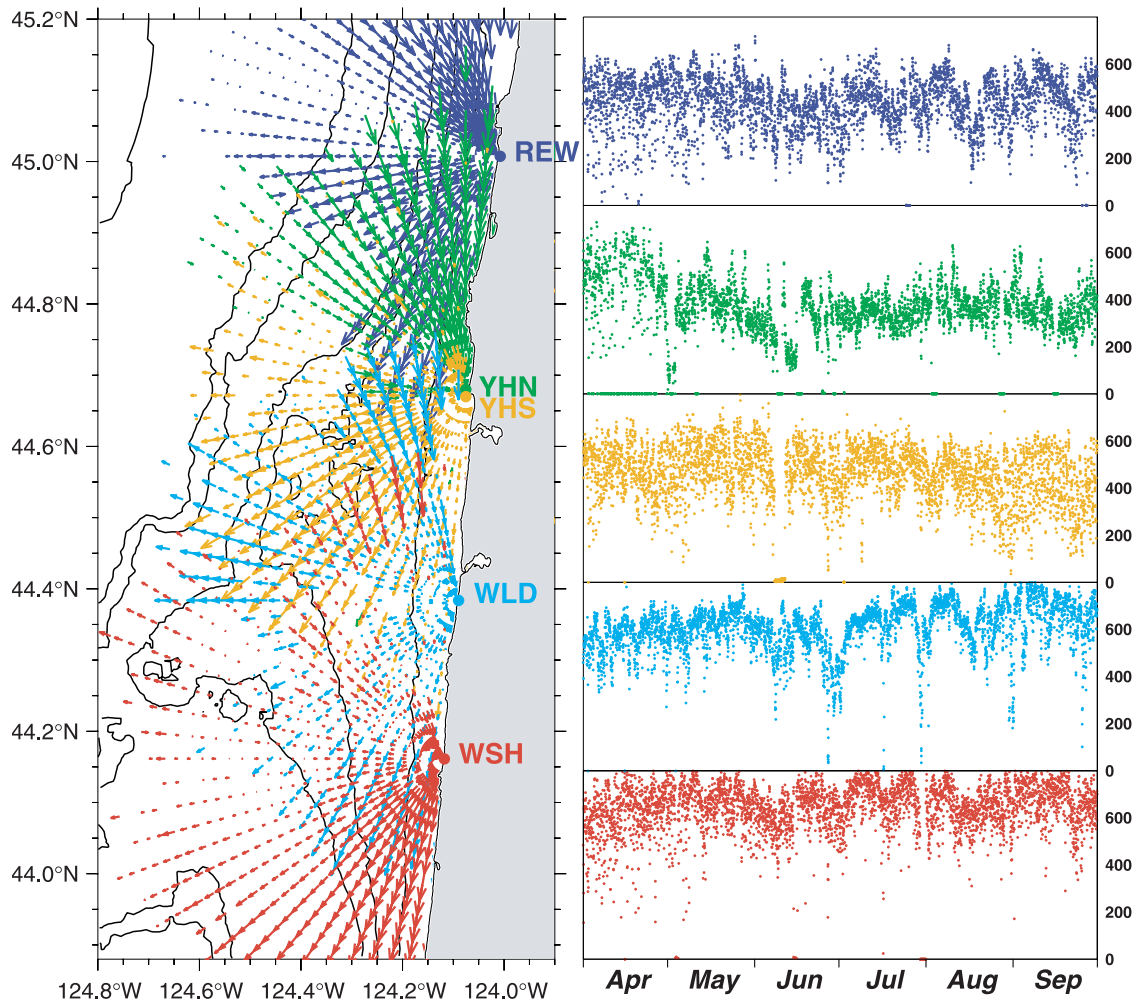


**Figure 2.** (left) Radial currents measured from each of the five HF sites during a single hour (10 May 2001, 1000 UTC). Bathymetric contours at 50 m, 80 m, 100 m, 150 m, 200 m, and 500 m are shown. (right) Timeline for April–September, 2001, showing number of radial measurements per hour at each site.

using the manufacturer’s software, to provide daily averaged maps to the sea-going elements of COAST, to help guide sampling.

[8] Wind measurements were obtained from two sites operated by the National Data Buoy Center: the Stonewall Bank buoy (NDBC 46050) at 44.62°N, 124.53°W, at the 130-m isobath near the Newport Hydrographic Line, and the shore-based CMAN station at Newport, Oregon (NWPO3), at 44.61°N, 124.07°W. An additional meteorological buoy was deployed for COAST at 45.00°N, 124.12°W, collecting data from 15 March through 28

August 2001 [Boyd *et al.*, 2002]. Wind stress was computed by correcting the hourly measurements to 10 m height and using the bulk coefficients of *Large and Pond* [1981].

[9] Measurements from the tide gauge at South Beach, Oregon (ID 9435380, 44.63°N, 124.04°W), operated by the National Ocean Service of NOAA, and modeled atmospheric pressure from the NCEP reanalysis, were detided and used to compute seasonally and atmospherically adjusted coastal sea level anomalies, following *Kosro* [2002]. In the following, all time series data have been low-pass filtered with a cosine-Lanczos, 46-hour half-power point filter, to remove

**Table 1.** Site Designators, Names, Locations, and Frequencies

Designator	Site Location	Latitude	Longitude	Frequency, MHz
REW	Road’s End Wayside	45° 00.45’ N	124° 00.44’ W	12.18
YHN	Yaquina Head North	44° 40.61’ N	124° 04.53’ W	13.51
YHS	Yaquina Head South	44° 40.30’ N	124° 04.52’ W	12.14
WLD	Waldport/Beachside	44° 23.03’ N	124° 05.38’ W	13.43
WSH	Washburne State Park	44° 09.69’ N	124° 07.05’ W	12.22

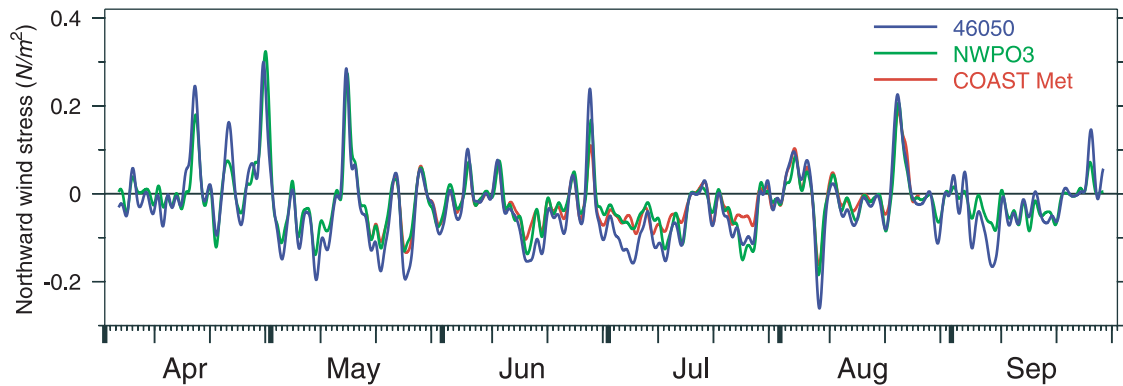


**Figure 3.** Northward wind stress  $\tau^y$  ( $\text{N/m}^2$ ) at three locations shown in Figure 1: buoy 46050 (blue,  $44.62^\circ\text{N}$ ,  $124.53^\circ\text{W}$ ), coastal C-MAN station NWPO3 (green,  $44.61^\circ\text{N}$ ,  $124.12^\circ\text{W}$ ), and the COAST meteorological mooring (red,  $45.00^\circ\text{N}$ ,  $124.12^\circ\text{W}$ ). Hourly wind stress has been low-pass filtered with a half-power point of 46 hours. Note that low-pass-filtered data from COAST meteorological mooring are available only for 18 May to 26 August.

tidal and inertial signals and emphasize the sub-inertial forcing and response [Moore *et al.*, 1968; Beardsley *et al.*, 1985].

### 3. Results

[10] An examination of coastal sea level, adjusted for atmospheric pressure, indicates that the drop associated with the spring transition to upwelling occurred on 10 March 2001, and the rise associated with the fall transition occurred on 12 November 2001. Therefore the entire study period, April through September 2001, is during the spring/summer season.

[11] Winds measured near the shelf edge, at NDBC buoy 46050, during April–September 2001 were upwelling favorable on average, imposing a mean surface stress of  $0.031 \text{ N/m}^2$ , directed east of south, toward  $153^\circ\text{T}$ . However, wind fluctuations were considerably stronger than the mean, and periods of downwelling-favorable wind forcing alternated with periods of upwelling favorable forcing (Figure 3), with northward wind stress present 29% of the time. The duration of the downwelling wind episodes was shorter, on average, than the periods of upwelling-favorable winds, being forced by transient storms. Bane *et al.* [2005] discuss how the downwelling storms are modulated at intraseasonal timescales of  $O(20 \text{ days})$  by north/south motion of the jet stream. Wind fluctuations at buoy 46050 were strongly polarized nearly north-south, along  $357.3^\circ\text{T}$ , with stress along the major axis being 4 times as large as along the minor axis ( $0.080 \text{ N/m}^2$  vs.  $0.020 \text{ N/m}^2$ , respectively).

[12] Measured northward wind stresses from the other anemometers, on the shore (NWPO3) and over the northern shelf (COAST), were highly correlated with those at NDBC 46050, (0.93 and 0.96, respectively). The strength of the subinertial northward wind fluctuations was somewhat weaker at the shore and over the northern shelf (standard deviations of  $0.063 \text{ N/m}^2$  at NWPO3 and  $0.053 \text{ N/m}^2$  at COAST, compared with  $0.080 \text{ N/m}^2$  at 46050). Correlations indicate that lags between fluctuations at the various anemometers, if any, were short: less than 3 hours.

#### 3.1. Pulsed Upwelling and Downwelling

[13] A map sequence from May (Figure 4) shows the time-varying structure of the coastal surface currents early in the upwelling season, in response to the reversing alongshore winds. A 3-day downwelling wind event (13 May 1300 to 16 May, 2000 UTC; Figure 4a) with peak winds of  $0.30 \text{ N/m}^2$  on 14 May, 1500 UTC, was followed by 6-days of upwelling-favorable winds (16 May 2000 to 22 May, 2100 UTC; intermediate peaks of  $-0.13 \text{ N/m}^2$  and  $-0.18 \text{ N/m}^2$  on 19 May 0500 and 20 May, 2100 UTC, respectively). A brief wind reversal (22 May, 2100 to 24 May, 0400 UTC, peak northward winds of  $0.05 \text{ N/m}^2$  on 23 May at 1400 UTC) followed, before winds turned upwelling favorable for another 3 days (24 May 0400 to 27 May 0700 UTC, peak winds of  $-0.20 \text{ N/m}^2$  on 25 May 0700 UTC). The ocean response is shown near the peak of the first downwelling wind event (Figure 4b), during the light winds (Figure 4c), at the peaks of upwelling winds (Figures 4d and 4e), during the brief wind reversal (Figure 4f) and during the peak upwelling winds that followed (Figure 4g).

[14] The response to the strong downwelling event has onshore surface flow at all locations, with poleward currents strongly predominating over equatorward currents (Figure 4b); median currents are  $16.0 \text{ cm/s}$  eastward and  $5.7 \text{ cm/s}$  northward. There is a strong tendency for the poleward flow to be enhanced near the coast. For example, along  $44.3^\circ\text{N}$  near the coast, the northward component increases from  $-27$  to  $33 \text{ cm/s}$  over  $26 \text{ km}$ , providing a relative vorticity of  $0.2 \times 10^{-4} \text{ s}^{-1}$  ( $0.2f$ ).

[15] As the winds pass through zero from downwelling-favorable to upwelling favorable (Figure 4c), the surface currents generally weaken in magnitude. Even before the winds have reversed, the mean alongshore flow becomes equatorward, with indications of the formation of an along-shore coastal jet, particularly north of Cape Foulweather. A cyclonic eddy forms near  $44.2^\circ\text{N}$ ,  $124.4^\circ\text{W}$ , about  $20 \text{ km}$  wide, centered in  $90 \text{ m}$  water depth, with positive relative vorticity of  $0.15 \times 10^{-4} \text{ s}^{-1}$ .

[16] As the upwelling-favorable wind forcing increases from late on 16 May through late on 20 May, the surface

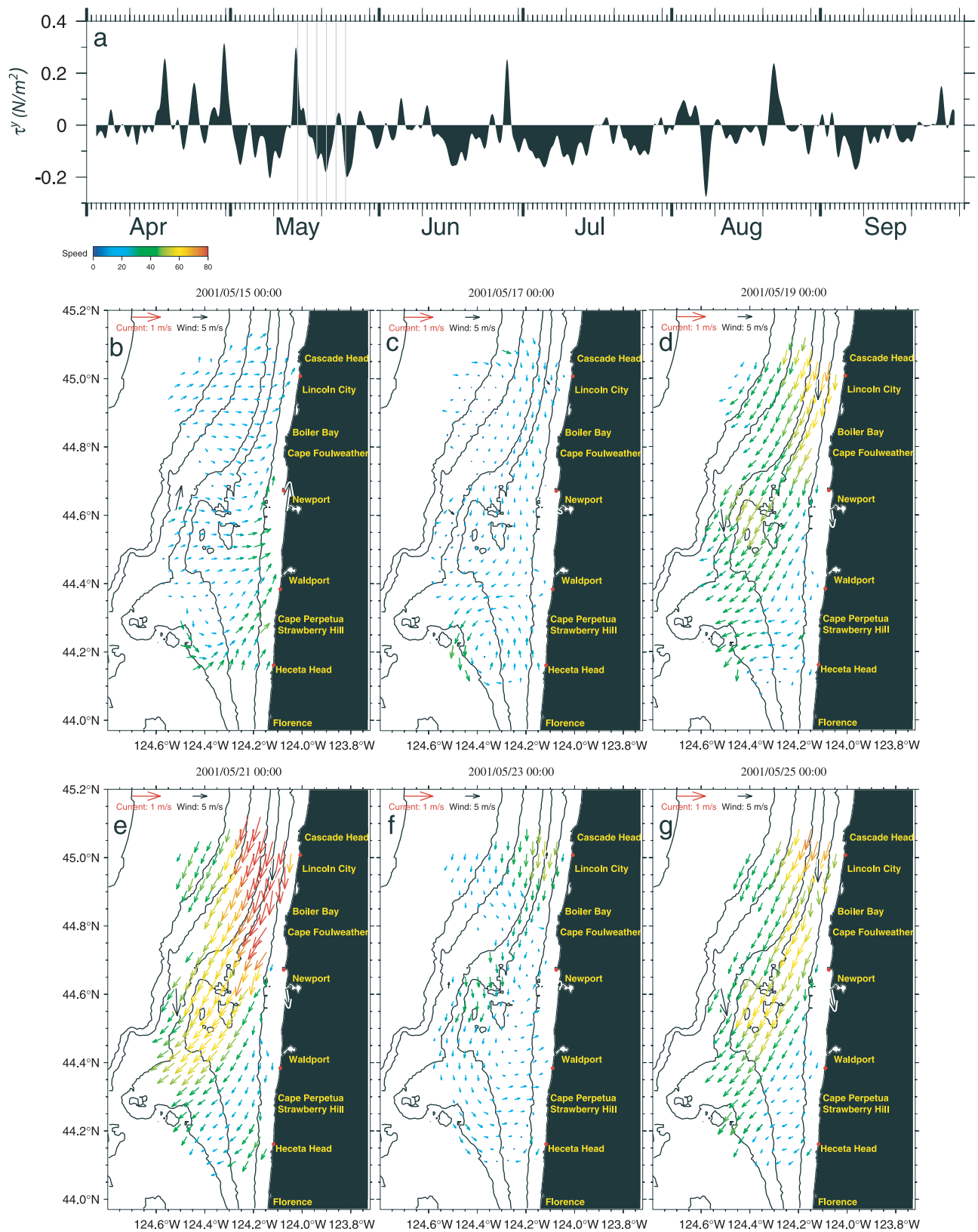


**Figure 4.** Time series maps of surface currents during May 2001. (a) The 10-m wind stress (N/m<sup>2</sup>) estimated from NDBC buoy 46050. Gray lines indicate times of the maps shown in Figures 4b–4g. Maps show subinertial surface currents, with speeds color coded, and measured winds at up to three buoys (black arrows). Data density has been reduced by a factor of 4 from the initial estimation grid, for clarity.

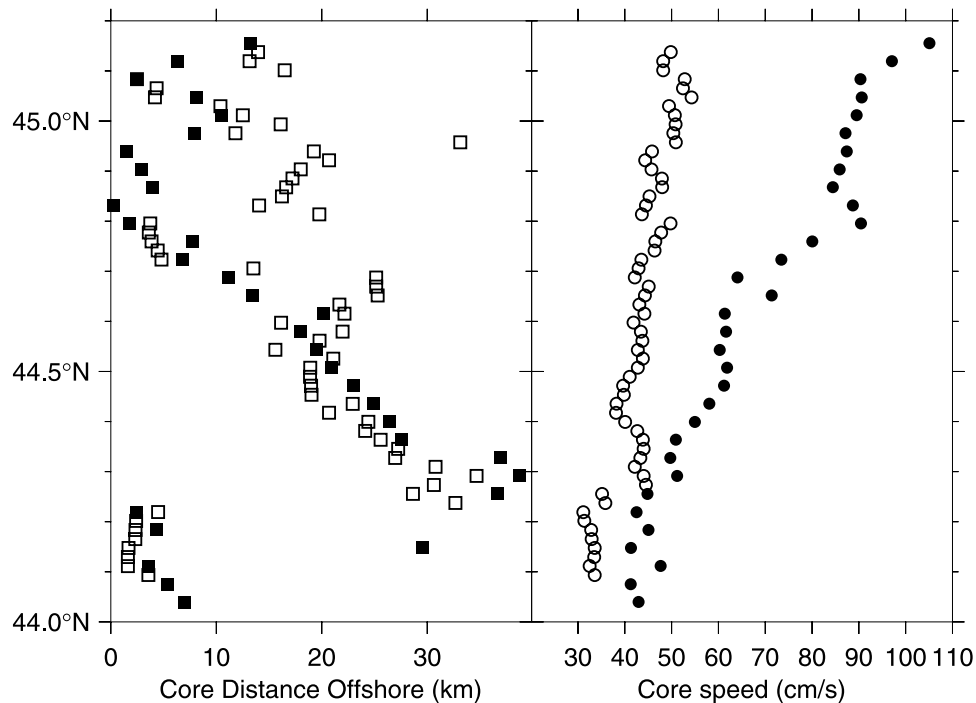


**Figure 5.** (right) Location of the core of the equatorward jet, and (left) speed at core location, for the maps from 21 May 2001 (solid symbols) and Aug 8, 2001 (open symbols). Near 44.2°N, a new jet core appears nearshore, moving offshore with distance to the south.

currents form an alongshore jet, flowing equatorward (Figures 4d and 4e). The dominant current direction on May 19 is toward the southwest; the median current direction is 213°T, and 80% of the current vectors point within 30° of the median. The core speeds in the jet were about 65 cm/s north of Cape Foulweather, with the core centered near the coast (within 10 km). South of Cape Foulweather, the jet core is found at increasing distances from the coast (reaching 30 km offshore near 44.3°N), the current direction has rotated to the west, and the core speeds generally decrease alongshore, except for a localized maximum above Stonewall Bank. Inshore of the main jet, currents are generally weak.

[17] By 21 May (Figure 4e), the currents during the peak upwelling-favorable winds were similar in structure to those from 19 May (Figure 4d), but with the strength of the equatorward alongshore jet increased substantially. Figure 5 examines the location and speed of the core of the equatorward jet on 21 May 2001 (solid symbols). North of Cape Foulweather, the jet core was within 12 km of the coast; south of Cape Foulweather, between 44.8°N and 44.4°N, the jet core lies increasingly farther offshore, nearly linearly with latitude, to 28 km offshore. The core speed decreased, again nearly linearly with latitude, from 105 cm/s at 45.16°N to 55 cm/s at 44.4°N. As the main jet is carried farther from shore, a second equatorward jet spins up at the coast, beginning near 44.2°N (Figure 5a). Its offshore core location (Figure 5a) and width (Figure 4e) both appear to increase southward as well.

[18] The weak wind reversal on 23 May decelerates, but does not erase, the main jet (Figure 4f). The equatorward core can still be traced from 45.1°N to 44.6°N (Newport), following the 80-m isobath, with strongest equatorward

flow still found north of Cape Foulweather. A remnant of the southern, nearshore jet can still be seen near Heceta Head. Near the coast south of Newport, the flow has begun to show characteristic downwelling properties – poleward, shoreward, and coastally enhanced. Cyclonic rotation of the onshore flow south of 44.4°N, similar to that present in the earlier downwelling event (Figures 4b and 4c) can be seen. With the return of stronger upwelling favorable winds on May 25 (Figure 4g), the equatorward coastal jet quickly begins to re-establish itself.

### 3.2. A Sustained Wind Reversal

[19] Wind conditions for August 2001 (Figure 6a), during the second set of cruises, were milder than during the first set (May–June 2001), aside from two moderate events. Between 2000 UTC on 6 August and 1900 UTC on 9 August, an upwelling-favorable wind event was measured at NDBC 46050, with peak northward wind stress of  $-0.28 \text{ N/m}^2$  at 0300 UTC on 8 August. Mild, generally upwelling-favorable winds were present for the next 11 days until a downwelling-favorable wind event, from 2300 UTC on 20 August through 1900 UTC on 24 August, reached peak northward wind stress of  $0.24 \text{ N/m}^2$  at 07:00 UTC on 22 August.

[20] The response to the 8 August upwelling-favorable wind event was similar to, though weaker and broader than, the response to the wind event of 21 May (Figure 4b; Figure 6b), with an equatorward alongshore current whose core is near the coast north of Cape Foulweather, and angles offshore south of Cape Foulweather. In the north, the core speed of the surface current is less than half its value in May (Figure 5), and the core maximum is less pronounced (currents are more uniform across current). The near uni-

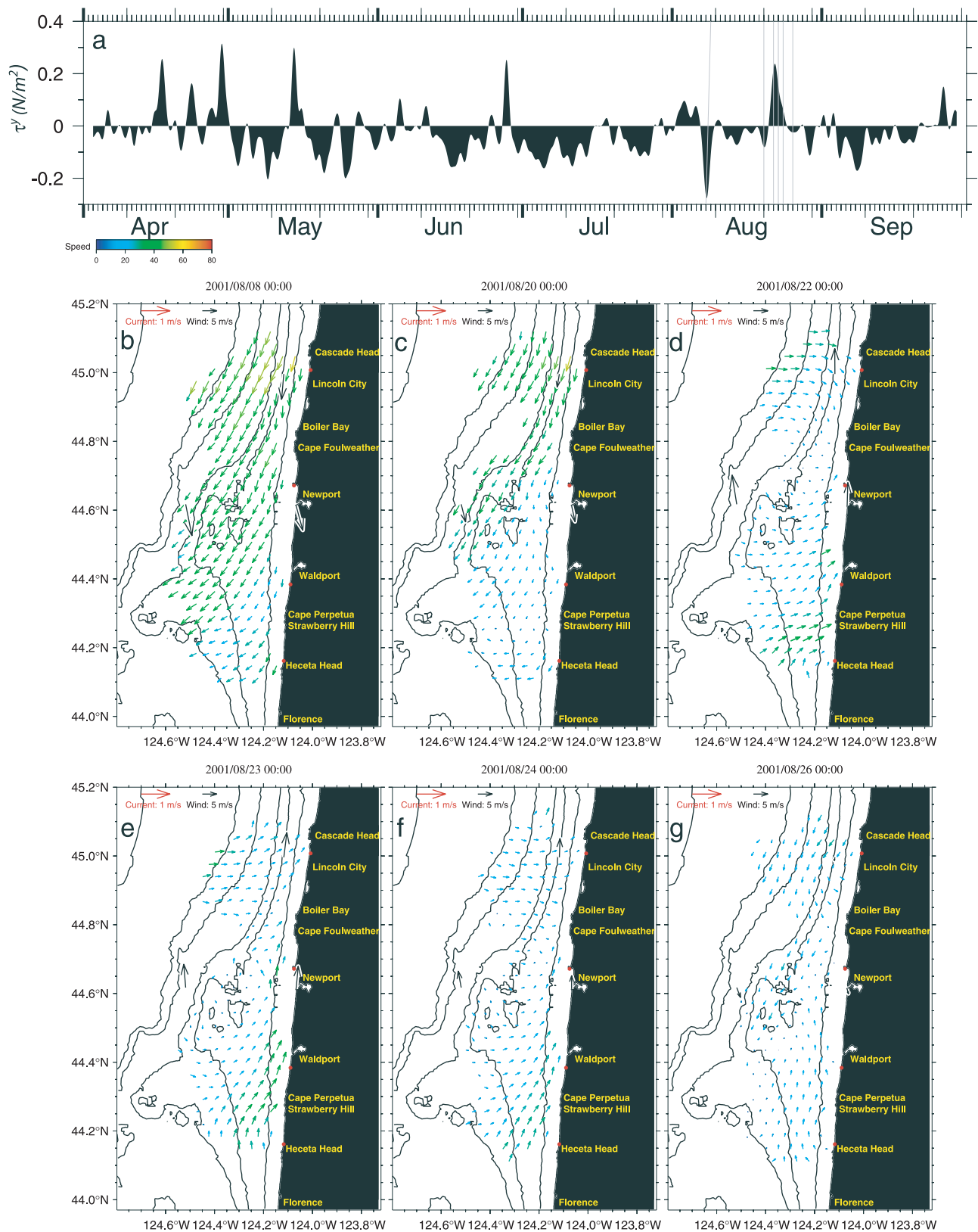


**Figure 6.** Time series maps of surface currents during August 2001. (a) The 10-m wind stress (N/m<sup>2</sup>) estimated from NDBC buoy 46050. Gray lines indicate times of the maps shown in Figures 6b–6g. Maps show subinertial surface currents, with speeds color coded, and measured winds at up to three buoys (black arrows). Data density has been reduced by a factor of 4 from the initial estimation grid, for clarity.

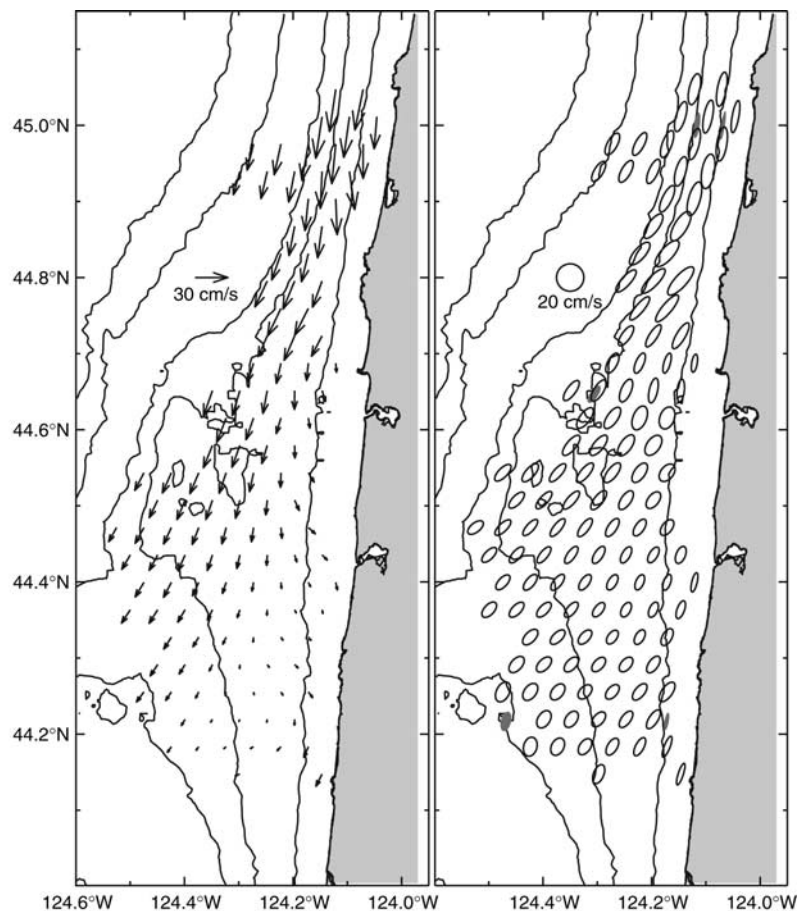


**Figure 7.** (left) Average currents and (right) fluctuation ellipses for period April through September 2001 in the COAST region, measured by HF surface current array. Ellipses are resolved along the principal axes of the subinertial current fluctuations. Fluctuations at 10 m from moored current meters are shown as five shaded ellipses. Isobaths shown are 50 m, 80 m, 100 m, 150 m, and 200 m.

formity of the currents across jet leads to noise in determination of the core locations north of Cape Foulweather (Figure 5a). South of Cape Foulweather, however, there is a striking similarity in the core positions for both wind events, as the core of the jet moves offshore between 44.8°N and 44.25°N, and as a second, southern jet spins up south of 44.25°N. As in May, the core speed in August tends to decrease from north to south, trending from 50 cm/s near 45.1°N to about 40 cm/s near 44.25°N.

[21] The weak winds preceding 20 August produced a weaker equatorward coastal jet, with much weaker flow inshore of the jet (Figure 6c). As the wind reversal event centered on 22 August passes through (Figure 6d), currents are onshore and, south of Cape Foulweather, poleward in a wedge-shaped sector widest in the south. By 23 August (Figure 6e), the currents nearshore have become oriented more poleward both north and south of Cape Foulweather, and this continues on the following day (Figure 6f), though current magnitudes decrease along with the wind stress. By 26 August (Figure 6g), very weak southward winds have begun to re-establish the equatorward jet north of Cape Foulweather, while currents in the south remain very weakly poleward.

[22] The downwelling front produced by this wind event was resolved with several high-resolution hydrographic

sections by M. Ott et al. (Summertime downwelling off the Oregon coast, submitted to *Journal of Geophysical Research*, 2005), who also find enhanced mixing near the downwelling front with collocated microstructure measurements. They propose a 2-day lag time to establish the downwelling front; this is longer than found with the HF for surface current response to wind forcing in this region (see below).

### 3.3. Overall Averages and Fluctuations

[23] Maps of surface current averages and fluctuations for April through September 2001 are shown in Figure 7. The equatorward alongshore coastal jet dominates the average map. North of Cape Foulweather, between 45.1°N and 44.8°N, the average jet is strong ( $O(40\text{ cm/s})$ ), centered close to shore ( $O(124.1^\circ\text{W})$ ), and directed nearly along isobath, toward about  $185^\circ\text{T}$ . Farther south, near Cape Foulweather, the flow turns offshore with the isobaths, toward about  $201^\circ\text{T}$ . Between 44.8°N and 44.5°N, the average core speed decreases to  $O(20\text{--}25\text{ cm/s})$ , and the core moves farther offshore toward Stonewall Bank. South of about 44.5°N, by contrast, the 80-m and 100-m isobaths trend closer to shore, but the average surface equatorward jet continues to the southwest, now crossing the isobaths at a steep angle. The inner edge of the average jet can be seen migrating farther offshore to the south below 44.3°N, as the core of the jet

probably moves beyond the range of the HF mapper. An additional feature of the mean field is a nearshore wedge of weak average flow, found inshore of the jet and south of Cape Foulweather. South of 44.2°N and inshore of the 50-m isobath, there is an indication in Figure 7 that a second average equatorward current jet develops near the coast.

[24] The subinertial alongshore current fluctuations (those along the major principle axis) tend to be strongest in the north and nearshore, with the strongest values, greater than 26 cm/s, just north of Cape Foulweather (Figure 7). The core of strongest alongshore fluctuations trends to the southwest, decreasing in strength; the weakest alongshore fluctuations are found near 44.35°N, 124.25°W. By contrast, the cross-shore current fluctuations are more uniform in magnitude, generally 5–8 cm/s.

[25] The subtidal fluctuations in surface currents also have a polarization with the major axis nearly aligned with the bottom topography north of about 44.5°N. Farther south, between 44.5°N and 44.2°N, the major axis of fluctuations includes a sizable cross-isobath component (Figure 7). North of 44.5°N, the weak cross-isobath orientation of the surface fluctuations is shoreward during poleward flow and offshore during equatorward, as expected for wind-driven currents on the eastern margin. The polarization of the low-frequency fluctuations is strongest near the coast north of Cape Foulweather, with standard deviations along the major axis typically 2.8 to 4 times those along the minor axis (Figure 7). Higher polarization tends to follow the jet axis, with higher values farther from shore over Stonewall Bank. Overall there is a trend toward decreasing polarization to the southwest, falling well below 2 in the offshore waters south of 44.3°N. Polarization increases inshore near 44.2°N, where the secondary equatorward jet was observed. Using data from moored current meters over the shelf between 44.6°N and 45.6°N, *Kundu and Allen* [1976] noted the tendency for vertically averaged, subinertial current fluctuations to be polarized along the topography; their observations did not extend south of 44.5°N, where the strongly cross-isobath surface fluctuations were observed in this study.

### 3.4. Synoptic Fluctuations

[26] To examine the behavior of the alongshore jet, an along-jet coordinate system was defined using the major axis of the low-frequency fluctuations. This direction varies with location both across shelf and along shelf (Figure 7). For this study, four latitudes (44.2°N, 44.4°N, 44.6°N and 45.0°N) were selected for analysis (44.8°N was skipped, as the cross-shelf coverage there is limited). A linear fit was made to the longitudinal variation of the major-axis orientation with location, and the currents were resolved along this direction. The resulting along-jet currents are shown in Figure 8 as a longitude-time plot for the four latitudes. In addition, the core location and strength of the strongest poleward and/or equatorward jet were estimated at each latitude and time, using a minimum speed threshold of 15 cm/s. The northward wind velocity from NDBC 46050 is also shown.

[27] The alternation in time of equatorward and poleward jets dominates the variability in the alongshore surface currents in Figure 8. The alongshore coherence of these fluctuations is generally high, with many reversals apparent

and coincident at all latitudes; examples include poleward current events centered near day 107, 120, 135, and 235, and equatorward events centered near day 140, 145, 151, and 220. The timing and direction of the current fluctuations generally reflect the wind forcing (Figure 8, left).

[28] However, alongshore differences are also apparent. There is a marked tendency for stronger and more frequent equatorward currents in the north (where the shelf is narrow and isobaths straight) than in the south (where the shelf widens and isobaths trend offshore), while poleward currents are more intense and of longer duration south of Cape Foulweather. Nearshore-trapped reversals to poleward flow, occurring during poleward wind events, were rarely seen at 45.0°N, especially during the period from day 140 to 210 (20 May to 29 July); they tended to be extend a shorter distance offshore at the intermediate latitudes (44.6°N and 44.4°N) than at the most southern latitude (44.2°N), where the shelf is widest.

### 3.5. Equatorward and Poleward Jets

[29] The time-varying longitude of the jet cores are shown as red (blue) dots in Figure 8 for the strongest equatorward (poleward) current that exceeds 15 cm/s. The core of the synoptic equatorward jet tends to be found at increasing distance from shore from north to south. The offshore branch of the equatorward jet is usually within the view of the HF mapping array at the two northern latitudes, but is often not seen at the two southern latitudes, presumably because it has traveled offshore from the mapped region. The second, inshore equatorward jet is most apparent at the southern latitude 44.2°N, indicated by the numerous equatorward core locations (red dots) found near 124.1°W–124.2°W; this branch is also evident, though less frequent, along 44.4°N, and is intermittently, and briefly, seen as far north as 44.6°N (e.g., days 112, 248, and 255).

[30] The behavior of the poleward jets is simpler (Figure 8, cores at blue dots). These jets tend to be coastally intensified, with cores most often at the shoreward longitude, particularly at the more northern latitudes where the shelf is narrowest. As the shelf widens in the south, at 44.4°N and 44.2°N, the probability increases that the strongest poleward flow will be found away from the coast. At 44.2°N, the poleward core is typically found detached from the coast, for example, near 124.25°W for sustained periods around days 215 and 235 (during periods of strong, sustained poleward winds).

[31] When the locations of the jet cores across 44.6°N are displayed as a histogram (Figure 9), it is clear that the distributions of the poleward and equatorward jets are much different. The strongest poleward currents at this latitude are nearly always found at the most inshore mapped location, exhibiting very little cross-shore migration. The core of the strongest equatorward current past 44.6°N, on the other hand, is centered most often near mid-shelf, with a mean longitude of 123.35°W, with a standard deviation of 6 km. There is a substantial gap in the distribution of equatorward jet cores over the inner 8 km (0.1 degree of longitude); after tidal and other high-frequency variability have been filtered, the equatorward jet is very rarely seen inshore of 124.2°W, despite the frequent reversals of the wind direction and the response of the currents. This impression is of a surface jet that spins up more or less in place, rather than migrating

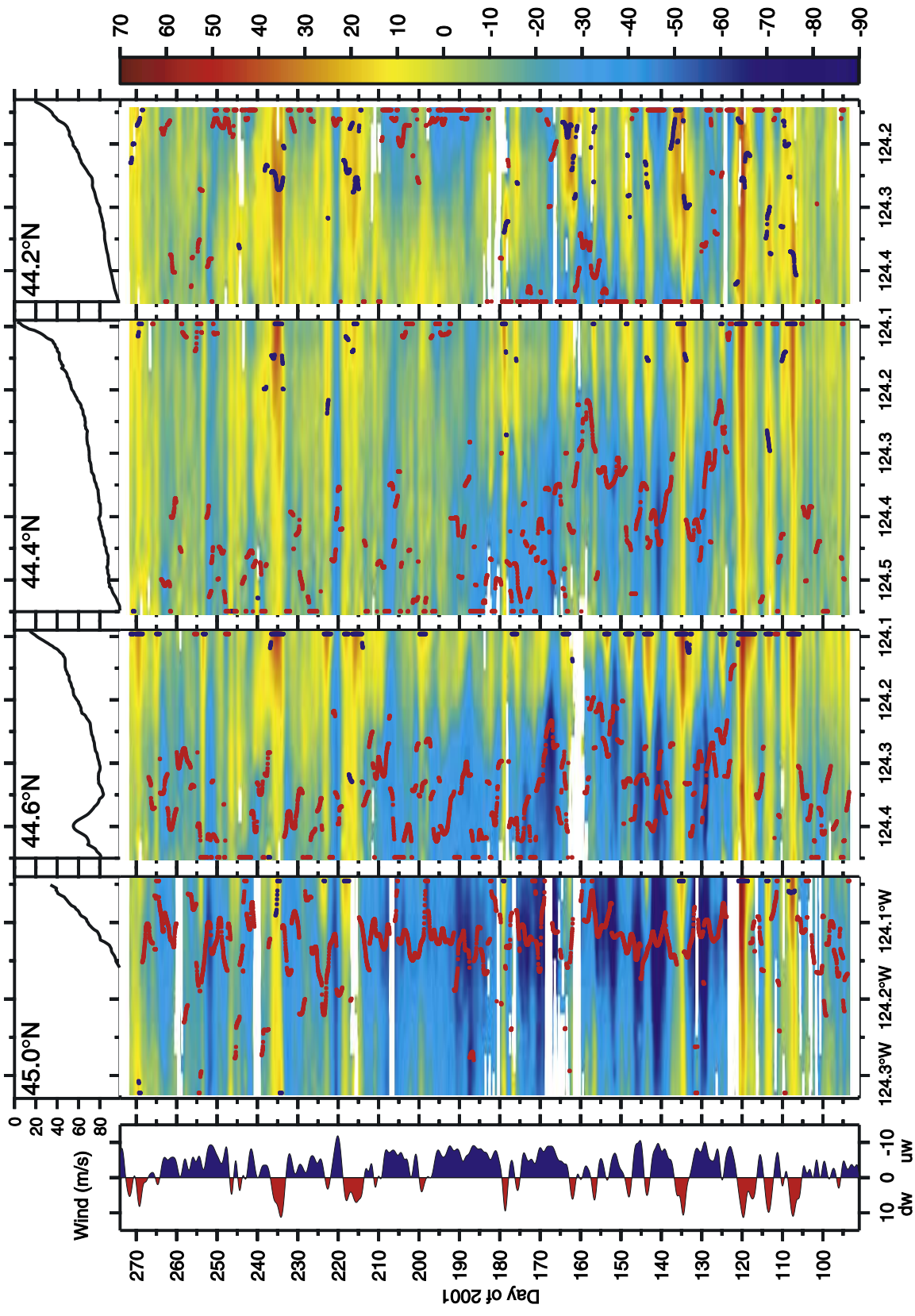
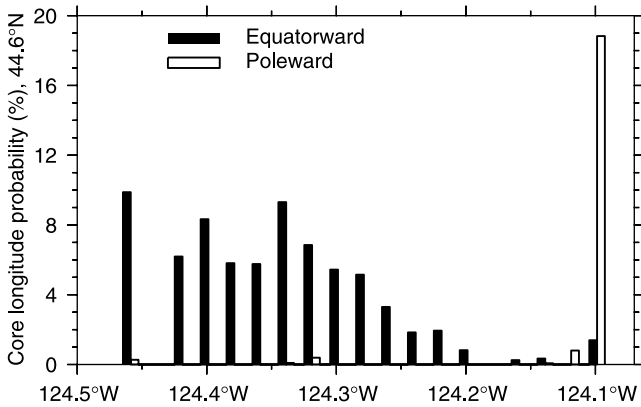


Figure 8. Surface alongshore current as a function of time is shown on four east-west transects. Locations of strongest equatorward (poleward) jet exceeding 15 cm/s in strength are shown as red (blue) dots. Northward wind component at NDBC buoy 46050 (44.62°N, 124.53°W) is shown at left. The cross-shore profile of bottom depth is shown above each transect.



**Figure 9.** Histogram of longitudes for equatorward (black) and poleward (white) jet cores across section at 44.6°N.

across the shelf with each wind reversal. This contrasts with the behavior of individual surface isotherms, which are observed to transit across the shelf during spin-up and spin-down, but possibly not with the formation of these isotherms into a surface front [Halpern, 1976].

[32] The strength of the jet cores is correlated with the strength of the northward wind stress at three of the four sections: 45.0°N, 44.6°N, and 44.4°N (0.6–0.7, at lags of 2–12 hours). However, the cross-shore location of the equatorward jet cores does not correlate with the strength of the northward wind stress. The use of integrated wind stresses over the recent past, as by Austin and Barth [2002], also did not produce a significant correlation with jet core location, for a wide range of filtering periods.

[33] When the jet core locations are resolved according to bottom depth rather than longitude (Figure 10), there is a tendency for the primary equatorward jet to be centered near the 80-m isobath at the three northern sections, with the secondary equatorward jet core appearing over the 25m isobath at 44.4°N and then over the 40-m isobath at 44.2°N. About 50% of the apparent dip in probability of finding the jet core at 75 m on 44.6°N is an artifact of the steep bottom gradients in this depth range.

[34] Counter to the tendency for the jet core location to be tied to topography, at 44.6°N the jet core can be seen

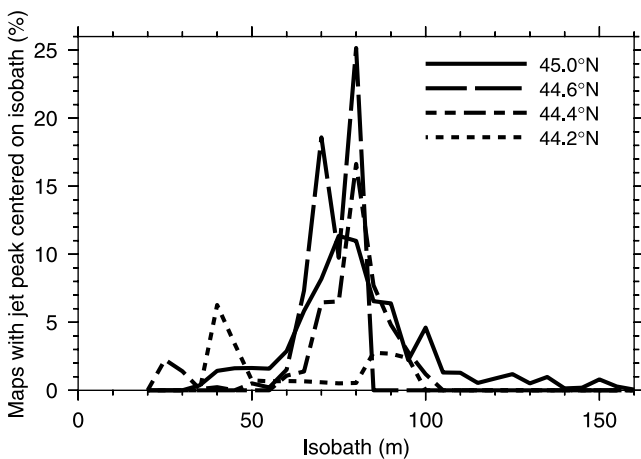


**Figure 10.** Histogram of locations for equatorward jet cores on each longitudinal section from Figure 8, by isobath.

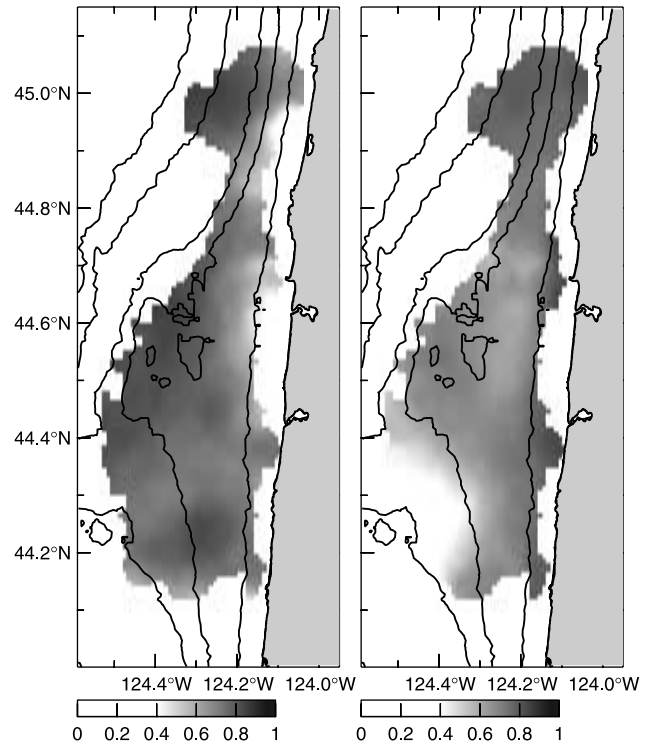


**Figure 11.** Correlation of northward wind stress  $\tau^y$  at NDBC 46050 with (left) eastward current  $u$  and (right) northward current  $v$ .

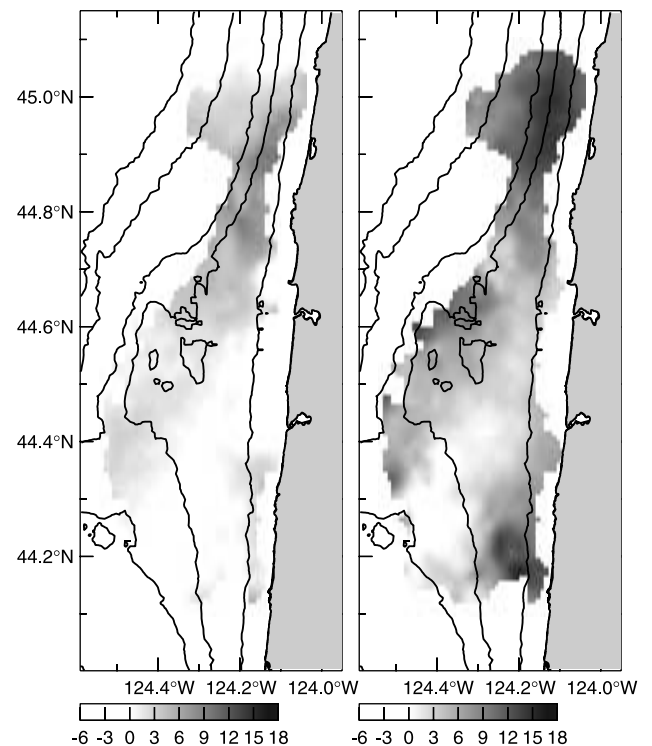


**Figure 12.** Lag in hours, by which currents (left)  $u$  and (right)  $v$  follow northward wind stress  $\tau^y$  at NDBC 46050, for maximum correlation.

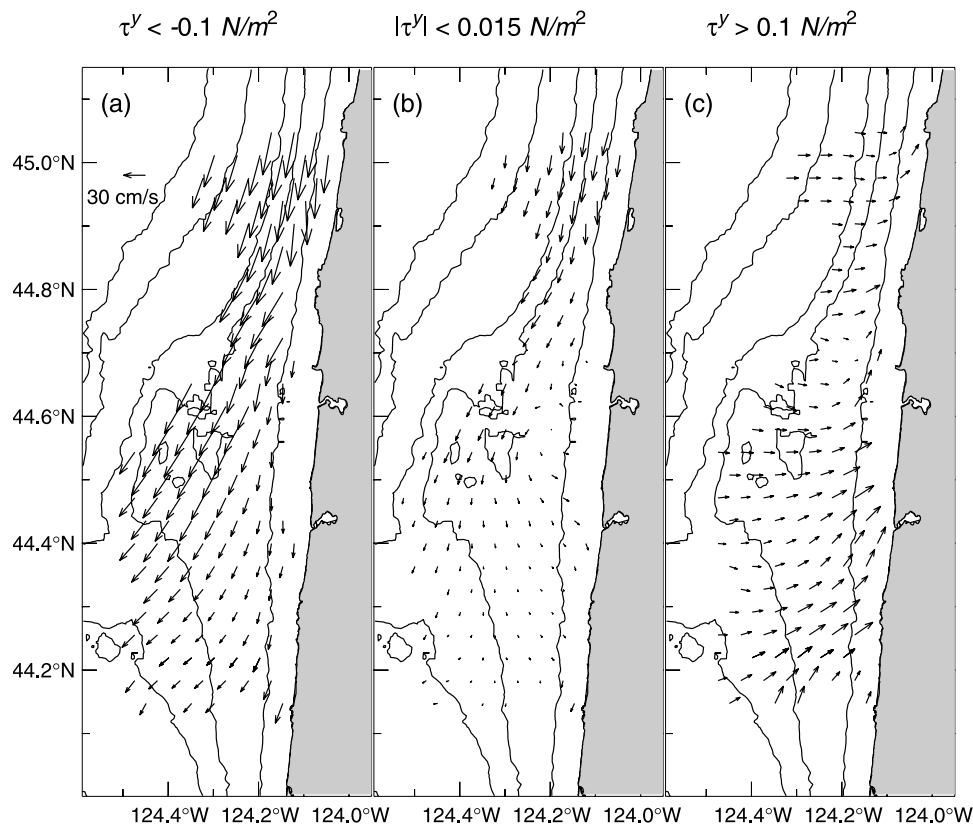


**Figure 13.** Average surface current during different wind forcing. (a) Strong equatorward wind stress ( $\tau^y \leq -0.1 \text{ N/m}^2$ ), (b) weak winds ( $|\tau^y| \leq 0.015 \text{ N/m}^2$ ), and (c) strong poleward wind stress ( $\tau^y \geq +0.1 \text{ N/m}^2$ ). Averages were made over periods where the low-pass filtered winds met the conditions for at least 24 hours.

migrating offshore during two prolonged wind events (Figure 8). From 16 June through 23 June (days 167 through 174), the core moves offshore some 15 km, from  $124.23^\circ\text{W}$  to  $124.42^\circ\text{W}$ , at an average speed of 2.4 cm/s. From 7 July through 14 July (days 188 through 195), the core moves offshore approximately 10 km, from  $124.30^\circ\text{W}$  to  $124.42^\circ\text{W}$ , at an average speed of 1.6 cm/s.

[35] The jet core also meanders on longer timescales south of Cape Foulweather (i.e., over the Heceta Bank complex). During the period centered on 7 June (day 158), the jet came into unusually shallow water at each section south of Cape Foulweather (Figure 8). This excursion was also noted by *Gan and Allen* [2005], from the results of their primitive equation model of the coastal circulation, during the period that they designate R1. A similar shoreward excursion can be seen in the HF data around 4 May (day 124). On a seasonal timescale, the jet core was more often found near the coast during spring than during summer (Figure 8). When the offshore jet was within view of the mapping array, its average location during 30 April through 23 June (days 120 through 174) was 5 km nearer shore at  $44.6^\circ\text{N}$  and 8 km nearer shore at  $44.4^\circ\text{N}$  than during 24 June through 30 September (days 175 through 273). This seasonal change in the jet trajectory also was noted by *Castelao and Barth* [2005], based primarily on moored time series data; they found that the offshore shift in the jet was accompanied by an increase in near-surface salinity at the shelfbreak mooring along

$44.2^\circ\text{N}$ , indicating the advance of the upwelling front farther from shore.

[36] As the shelf widens to the south around Heceta Bank, and the primary equatorward coastal jet moves farther from shore, we have noted above the presence of a lee region of weak surface flow inshore of the jet, along with a second, inshore equatorward jet, whose core also moves offshore to the south. In their model of the circulation over Heceta Bank, *Gan and Allen* [2005] obtain very similar structures in the time-mean surface flow (e.g., their Figure 10). Their modeled mean surface flow in the lee region is underlain by a current shear which further decreases the equatorward current with depth, eventually reversing it to poleward.

### 3.6. Relation to Winds

[37] To examine the spatially-varying relationship between subinertial winds and currents, the correlation between the northward wind stress at buoy 46050,  $\tau^y$ , and the eastward and northward components of surface current, ( $u$ ,  $v$ ), were computed (Figure 11), along with the time lag which maximized the correlation (Figure 12). The correlations were largely in the expected sense, with northward (southward) wind fluctuations associated with onshore (offshore) and poleward (equatorward) fluctuations in the currents. The strongest relation between  $\tau^y$  and  $v$  occurred near the coast, and in the narrow-shelf/simple topography region north of Cape Foulweather. There is a notable breakdown of the relationship between  $\tau^y$  and  $v$  in the far southwestern region, over Heceta

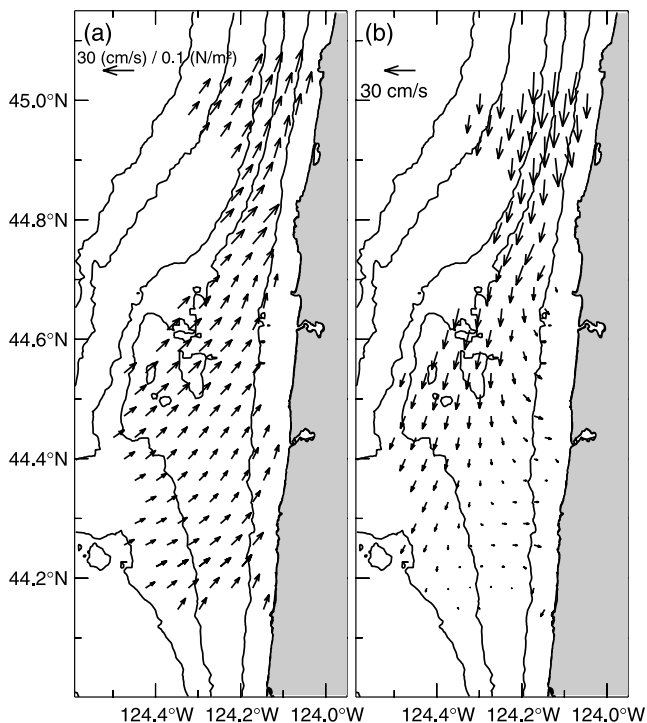


**Figure 14.** Linear regressions of the surface currents (cm/s) from the northward wind stress ( $\text{N/m}^2$ ) at NDBC buoy 46050 were computed, as a function of location. (a) Slope  $\vec{\alpha}$  ((cm/s)/(0.1  $\text{N/m}^2$ ), the increase in current per 0.1  $\text{N/m}^2$  increase in  $\tau^y$ , northward wind stress, and (b) intercept  $\vec{\beta}$  (cm/s), the predicted current at zero wind stress. Scale arrows indicate 30 (cm/s)/(0.1  $\text{N/m}^2$ ) and 30 cm/s, respectively.

Bank (e.g., 44.25°N, 124.4°W). Small eddies are repeatedly observed in this region of the shelf (e.g., Figures 4c and 4f, as well as EOFs 3 and 4 described later). Both of these are evidence that other mechanisms, such as interaction of the flow with the complex bathymetry in this region, are producing flow variations here [see also *Gan and Allen, 2005; Barth et al., 2005*].

[38] The time lag which produces the highest correlation between  $\tau^y$  and surface  $u$  or  $v$  is short, generally less than 12 hours and often less than 6 hours. The ocean response is typically faster across wind than downwind (Figure 12). Northward currents above Cape Foulweather are slower to respond to the wind than in most regions to the south. Similarly, longer lags are associated with the currents at the mean location of the jet. Although all lags have been computed relative to events at buoy 46050, recall that the time lag between winds at the three measured locations was generally 2 hours or less.

### 3.7. Averages During Strong and Weak Winds

[39] Patterns of flow during sustained strong and weak wind forcing were estimated (Figure 13) by computing conditional averages over periods of at least 24 hours duration during which the northward wind stress at NDBC 46050 either exceeded  $-0.1 \text{ N/m}^2$ , exceeded  $+0.1 \text{ N/m}^2$ , or were weaker than  $\pm 0.015 \text{ N/m}^2$ . Such periods accounted for approximately 17%, 6% and 9% of the record, respectively. The flow during strong southward winds (Figure 13a) shows

an equatorward jet with many of the same features as the overall average (Figure 7a), but with stronger southward flow evident, especially noticeable inshore of the jet, and with the near-coastal flow more shore-parallel. The second, inshore equatorward jet is seen nearshore below 44.2°N. Averages over the nine periods of weak winds lasting 24 to 105 hours show persistent residuals of the equatorward jets north of Cape Foulweather, over the outer shelf south of Cape Foulweather, and nearshore south of 44.2°N, with flow elsewhere generally weak (Figure 13b). The average surface currents during low winds were southward at all mapped locations (generally 50 m bottom depth or greater), except for a small region near 124.1°W, 44.6°N, where averages were weakly northward, averaging 0.9 cm/s. The average flow resulting from the five strong northward wind events which lasted at least 24 hours (Figure 13c) shows many features in common with the synoptic maps during the reversals of 15 May (Figure 4b) and 21–24 August (Figure 6).

### 3.8. Regressions With Alongshore Wind Stress

[40] For this experimental period, winds were measured at three locations during COAST (Figure 1). The meridional component had more than 90% of the subinertial kinetic energy, was correlated at 0.95 or higher between locations, and showed no significant time lags between buoys, while the RMS strength of the meridional winds were 5.69 m/s, 4.62 m/s and 4.50 m/s at the offshore buoy (46050), the northern buoy (COASTmet) and the shore CMAN station (NWPO3), respectively. To analyze the effect of wind forcing on the surface currents, we compute a linear regression between  $\tau^y$ , the northward component of the subinertial wind stress at NDBC 46050, and the subinertial surface currents:  $\vec{v}(x, y, t) = \vec{\alpha}(x, y)\tau^y(t) + \vec{\beta}(x, y)$ , where  $\vec{\alpha}(x, y)$  is the slope of the regression, giving the spatially dependent response of the surface currents to a variation in the meridional wind stress, and  $\vec{\beta}(x, y)$  is the intercept, giving the expected current when the meridional wind stress is zero. The results are shown in Figure 14.

[41] The sign of the regression slope  $\vec{\alpha}$  from  $\tau^y$  (Figure 14a) is positive everywhere, so that a poleward (equatorward) stress produces an increased poleward (equatorward) and onshore (offshore) current everywhere. However, the response varies spatially in magnitude, being 40% stronger north of Cape Foulweather (average magnitude 19.7 cm/s change in current per 0.1  $\text{N/m}^2$  change in  $\tau^y$ ) than south of Cape Foulweather (averaging 13.9 cm/s per 0.1  $\text{N/m}^2$ ). It also varies in direction, being more meridional (like the isobaths) above Cape Foulweather than below. Together, the combined effect produces a nearly fourfold change in meridional component of the response to  $\tau^y$  over the mapped region (20 cm/s per 0.1  $\text{N/m}^2$  in the north, 5 cm/s per 0.1  $\text{N/m}^2$  in the southwest). This is a much larger range of response (and with an opposite gradient) than expected based on the spatial variation in wind strength (Figure 3). We take this as evidence that the varying shelf width and bottom topography are modulating the strength of the current response. There is also an alongshore modulation in the cross-shore current response, with weaker response offshore from estuaries at the mouths of the Alsea (44.4°N), Yaquina (44.6°N) and Siletz (44.9°N) Rivers.

[42] The regression intercepts  $\vec{\beta}$  from  $\tau^y$  (Figure 14b; see also Figure 13b) show that, on average, the zero wind

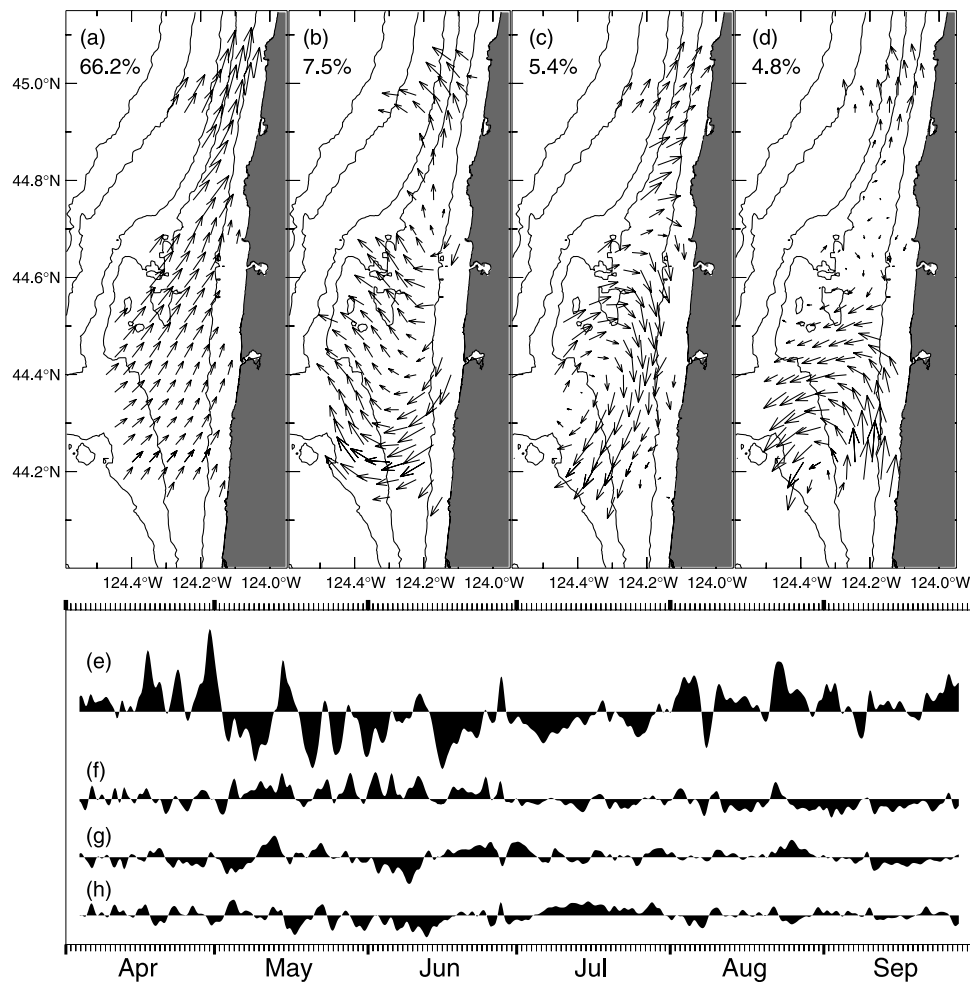


**Figure 15.** (a–d) Four most energetic empirical orthogonal modes of surface current variability, along with the percentage of total variance explained by each. (e–h) Time-varying amplitude of each empirical orthogonal mode.

condition is not accompanied by an absence of motion, but rather by a remnant equatorward coastal jet, strongest in the narrow shelf region north of Cape Foulweather, with low values being seen over an increasingly wide shelf region to the south. These results for  $\bar{\beta}$  contrast with those obtained off northern California during the Coastal Ocean Dynamics Experiment 2 (CODE2), where regression analyses showed that, in the absence of wind, vertically averaged flow was poleward at all shelf moorings [Winant *et al.*, 1987], and near-surface flow was poleward in 60 m and 90 m [Huyer and Kosro, 1987]. This suggests that the alongshore pressure gradient which develops counter to the wind is weaker, on average, off Newport than off northern California. In both Oregon and northern California, the surface equatorward coastal jet is a feature of the  $\bar{\beta}$  field farther out on the shelf.

### 3.9. EOFs

[43] Another view of the spatial patterns of time-varying currents is obtained using empirical orthogonal functions (EOFs) [Davis, 1976]. Two-thirds of the variance in the currents was accounted for by the first EOF (Figure 15a). This mode bears a strong resemblance to the linear response slope  $\vec{\alpha}$  of currents to meridional winds (Figure 14a)

discussed above. It is dominated by alongshore currents which are the same sign across the whole map, vary smoothly and weakly in the across-shore direction, and are stronger and more meridional north of Cape Foulweather. The cross-shore component is generally onshore for positive mode fluctuations, that is, when the phase of the fluctuation has poleward alongshore currents. The next three most energetic EOFs account for half of the remaining variance (7.5%, 5.0% and 4.5%, respectively). EOF2 (Figure 15b) is dominated by the cross-shore velocity component, which has the same sign over nearly the entire range; the alongshore component of EOF2 changes sign across shore, south of Cape Foulweather. The other two EOF modes explain less of the energy in the surface fluctuations, and are characterized by shorter length scales.

[44] The time amplitudes of these modes, scaled to reflect the variance explained, are shown in Figures 15e–15h. Over the full time period, the amplitude of any mode is uncorrelated with that of any other mode. However, there are periods of one to several weeks (e.g., mid-May through mid-June, during early August) where the first and second modes co-vary, in phase, through several short-lived upwelling-relaxation cycles. Mode 1 has a somewhat longer integral timescale (3.9 days) [Davis, 1976; Sciremammano,

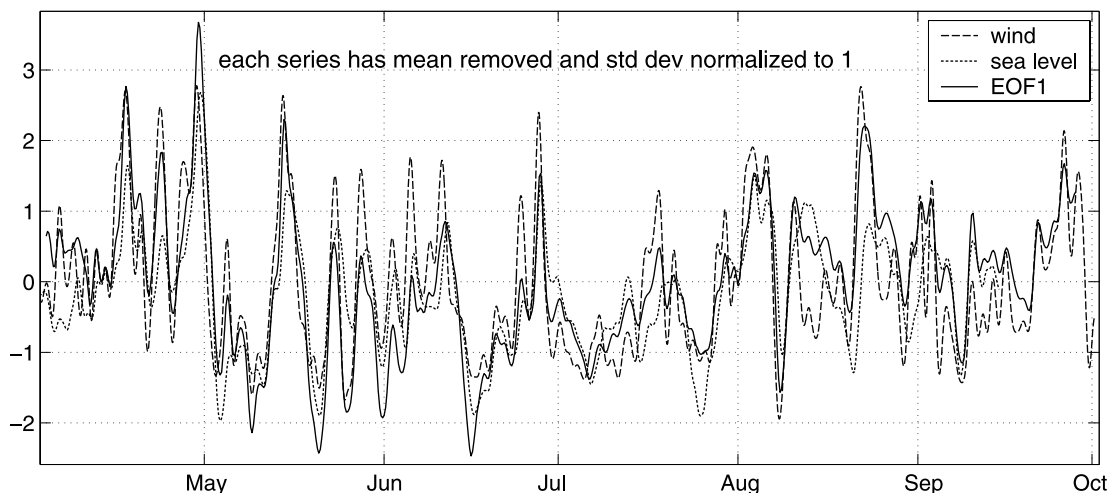


**Figure 16.** Time-varying amplitude of EOF1, of alongshore wind velocity (from NDBC 46050) and of sea level anomaly at Newport. Mean has been removed from each series, and each has been normalized to unit standard deviation.

1979] than the other three modes (2.5, 3.4 and 3.4 days, respectively).

### 3.10. Forcing

[45] The amplitude associated with mode 1 is strongly correlated with the northward wind stress  $\tau^y$  (Figure 16); the correlation is 0.83, with no significant lag. The correlation of this amplitude with coastal sea level at Newport (detided, low-pass filtered, adjusted for the inverse barometer effect) is also high (0.84 at zero lag) (Figure 16). Mode 2 is correlated at zero lag with the northward wind stress (0.39), but is uncorrelated with coastal sea level. Mode 3 is not significantly correlated with either the northward wind or with coastal sea level. Current fluctuations of mode 4 lag fluctuations in the wind by 1.75 days and lag fluctuations in sea level by 1.25 days; these correlations have similar strengths but opposite signs ( $-0.52$  for  $\tau^y$  and  $+0.50$  for sea level).

[46] The strong relationship between time-varying amplitude of mode 1 and the northward wind stress  $\tau^y$  extends over motions with periods of two or more days (Figure 17). The wind-driven portion of modes 2 and 4 involves motions with periods shorter than a week. Again, no significant coherence is seen with mode 3.

## 4. Conclusions

[47] A time series of well-resolved, remotely-sensed maps of surface currents has been used to examine the time-varying spatial structure of shelf currents off central Oregon, in a region of strongly non-uniform bathymetry, during the upwelling season of 2001. The wind forcing, varying between up- and down-welling favorable, produces a rapid response in the surface currents, and alternating flow states. An equatorward coastal jet, centered near the 80-m isobath between  $45.0^\circ\text{N}$  and at least  $44.4^\circ\text{N}$ , waxes and wanes with the intensity of the equatorward wind forcing, and persists through periods of zero equatorward wind. In this northern portion of the bank complex, the jet tends to follow the isobaths, with a core velocity which is strongest north of Cape Foulweather, where the shelf is narrow and straight.

The location of the equatorward jet core varies with time, but does not co-vary with the intensity of the equatorward wind. A second equatorward jet, previously unknown, develops near the coast as the shelf continues to widen south of  $44.5^\circ\text{N}$ , and the primary equatorward jet gets farther from shore. By contrast, south of  $44.5^\circ\text{N}$ , the average jet and its fluctuations were directed strongly across the 80-m and 100-m isobaths. During reversed winds, the surface currents south of Cape Foulweather reverse and form a coastally intensified poleward jet, whose core is coastally trapped at  $44.6^\circ\text{N}$ , but which has increasing probability of being detached from the coast where the shelf widens to the south. The time lag between the fluctuation in wind stress and the response of the surface currents is shorter than anticipated based on results from subsurface current-

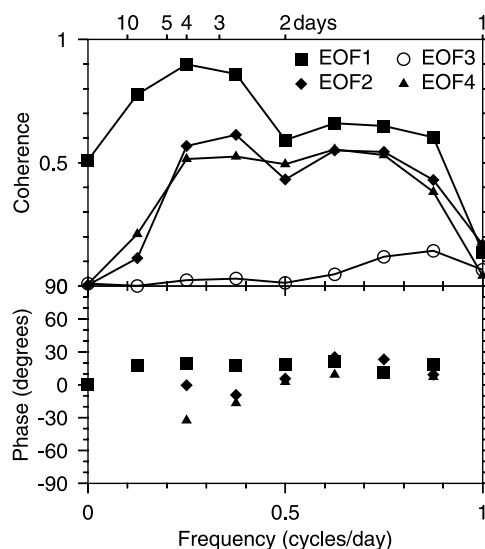


**Figure 17.** Cross-spectra, as coherence and phase, between the alongshore wind stress and the time-varying amplitude of each EOF; the estimated 95% confidence interval for coherence of 0.9 and 0.5 are  $\pm 0.03$  and  $\pm 0.21$ , respectively [Bendat and Piersol, 1993].

meters [Halpern, 1976]. The middle and outer shelf over Heceta Bank, in the south, is a region of low correlation between meridional wind forcing and meridional currents, indicating that other dynamics, such as small eddies and interactions with topography, are modifying the currents here. Wind stress varies coherently over the region, but is somewhat weaker north of Cape Foulweather and at the coast near Newport. However, the response of meridional currents to meridional wind stress varies spatially, and is up to 4 times stronger inshore, north of Cape Foulweather, than over Heceta Bank in the southwest corner of the study region.

[48] **Acknowledgments.** Thanks are given to W. Waldorf, D. Root, A. Dorkins, J. Simeon and S. O'Keefe for their contributions to the successful installation and operation of the HF array for COAST, to CODAR Ocean Sensors for their collaboration, and to J. Barth, J. Allen and P. Wheeler for their leadership of the COAST program. The manuscript benefited from comments by an anonymous reviewer and by the associate editor. This research was supported by the National Science Foundation, under grant 9907854.

## References

- Allen, J. S. (1973), Upwelling and coastal jets in a continuously stratified ocean, *J. Phys. Oceanogr.*, *3*, 245–257.
- Austin, J. A., and J. A. Barth (2002), Variation in the position of the upwelling front on the Oregon shelf, *J. Geophys. Res.*, *107*(C11), 3180, doi:10.1029/2001JC000858.
- Bane, J. M., M. D. Levine, R. M. Samelson, S. M. Haines, M. F. Meaux, N. Perlin, P. M. Kosro, and T. Boyd (2005), Atmospheric forcing of the Oregon coastal ocean during the 2001 upwelling season, *J. Geophys. Res.*, C10S02, doi:10.1029/2004JC002653.
- Barrick, D. E., and B. J. Lipa (1999), Using antenna patterns to improve the quality of SeaSonde HF radar surface current maps, paper presented at Sixth Working Conference on Current Measurement, Inst. of Electr. and Electron. Eng., San Diego, Calif.
- Barrick, D. E., M. W. Evans, and B. L. Weber (1977), Ocean surface currents mapped by radar, *Science*, *198*, 138–144.
- Barth, J. A., and R. L. Smith (1998), Separation of a coastal upwelling jet at Cape Blanco, Oregon, USA, *S. Afr. J. Mar. Sci.*, *19*, 5–14.
- Barth, J. A., and P. A. Wheeler (2005), Introduction to special section: Coastal Advances in Shelf Transport, *J. Geophys. Res.*, C10S01, doi:10.1029/2005JC003124.
- Barth, J. A., S. D. Pierce, and R. L. Smith (2000), A separating coastal upwelling jet at Cape Blanco, Oregon and its connection to the California Current System, *Deep Sea Res., Part II*, *47*(5–6), 783–810, doi:10.1016/S0967-0645(99)00127-7.
- Barth, J. A., S. D. Pierce, and R. M. Castelao (2005), Time-dependent, wind-driven flow over a shallow mid-shelf submarine bank, *J. Geophys. Res.*, C10S05, doi:10.1029/2004JC002761.
- Beardsley, R. C., R. Limeburner, and L. Rosenfeld (1985), Introduction to CODE-2 Moored Array and Large-Scale Data Report, in *CODE-2 Moored Array and Large-Scale Data Report, Tech. Rep. 85–35*, edited by R. Limeburner, pp. 1–22, Woods Hole Oceanogr. Inst., Woods Hole, Mass.
- Bendat, J. S., and A. G. Piersol (1993), *Engineering Applications of Correlation and Statistical Analysis*, Wiley-Intersci., Hoboken, N. J.
- Boyd, T., M. D. Levine, P. M. Kosro, S. R. Gard, and W. Waldorf (2002), Observations from moorings on the Oregon continental shelf, May–August 2001: A component of Coastal Advances in Shelf Transport (COAST), report, 196 pp., Coll. of Oceanic and Atmos. Sci., Oregon State Univ., Corvallis.
- Castelao, R. M., and J. A. Barth (2005), Coastal ocean response to summer upwelling favorable winds in a region of alongshore bottom topography variations off Oregon, *J. Geophys. Res.*, C10S04, doi:10.1029/2004JC002409.
- Chapman, R. D., L. K. Shay, H. C. Graber, J. B. Edson, A. Karachintsev, C. L. Trump, and D. B. Ross (1997), On the accuracy of HF radar surface current measurements: Intercomparisons with ship-based sensors, *J. Geophys. Res.*, *102*(C8), 18,737–18,748.
- Cook, M. S., and J. D. Paduan (2001), Processing HF Radar Data using the HFRadarnap Software System, in *Radiowave Oceanography: The First International Workshop*, edited by J. D. Paduan, pp. 12–16, Univ. of Miami, Timberline, Oregon.
- Davis, R. E. (1976), Predictability of sea surface temperature and sea level pressure anomalies over the North Pacific Ocean, *J. Phys. Oceanogr.*, *6*, 249–266.
- Davis, R. E. (1985), Drifter observations of coastal surface currents during CODE: The method and descriptive view, *J. Geophys. Res.*, *90*(C3), 4741–4755.
- Gan, J., and J. S. Allen (2005), Modeling upwelling circulation off the Oregon coast, *J. Geophys. Res.*, C10S07, doi:10.1029/2004JC002692.
- Gurgel, K.-W. (1994), Shipborne measurement of surface current fields by HF radar, *Onde Electr.*, *74*(5), 54–59.
- Halpern, D. (1976), Structure of a coastal upwelling event observed off Oregon during July 1973, *Deep Sea Res.*, *23*, 495–508.
- Huyer, A., and P. M. Kosro (1987), Mesoscale surveys over the shelf and slope in the upwelling region near Point Arena, California, *J. Geophys. Res.*, *92*(C2), 1655–1681.
- Huyer, A., R. D. Pillsbury, and R. L. Smith (1975), Seasonal variation of the alongshore velocity field over the continental shelf off Oregon, *Limnol. Oceanogr.*, *20*, 90–95.
- Huyer, A., E. J. C. Sobey, and R. L. Smith (1979), The spring transition in currents over the Oregon continental shelf, *J. Geophys. Res.*, *84*(C11), 6995–7011.
- Jones, B. H., and D. Halpern (1981), Biological and physical aspects of a coastal upwelling event observed during March–April 1974 off north-west Africa, *Deep Sea Res.*, *28*, 71–81.
- Kosro, P. M. (1987), Structure of the coastal current field off northern California during the Coastal Ocean Dynamics Experiment, *J. Geophys. Res.*, *92*(C2), 1637–1654.
- Kosro, P. M. (2002), A poleward jet and an equatorward undercurrent observed off Oregon and northern California, during the 1997–98 El Niño, *Prog. Oceanogr.*, *54*(1–4), 343–360.
- Kosro, P. M., and A. Huyer (1986), CTD and velocity surveys of seaward jets off northern California, July 1981 and 1982, *J. Geophys. Res.*, *91*(C6), 7680–7690.
- Kundu, P. K., and J. S. Allen (1976), Some three-dimensional characteristics of low-frequency current fluctuations near the Oregon coast, *J. Phys. Oceanogr.*, *6*, 181–199.
- Large, W. G., and S. Pond (1981), Open ocean momentum flux measurements in moderate to strong winds, *J. Phys. Oceanogr.*, *11*, 324–336.
- Lipa, B. J., and D. E. Barrick (1983), Least-squares methods for the extraction of surface currents from CODAR crossed-loop data: Application at ARSLOE, *IEEE J. Oceanic Eng.*, *8*, 226–253.
- Mooers, C. N. K., L. M. Bogert, R. L. Smith, and J. G. Patullo (1968), A compilation of observations from moored current meters and thermographs (and of complementary oceanographic and atmospheric data): Volume II—Oregon continental shelf, August–September 1966. *Data Rep. 30*, 98 pp., Dep. of Oceanogr., Oregon State Univ., Corvallis.
- Richards, F. A. (Ed.) (1981), *Coastal Upwelling, Coastal Estuarine Stud.*, vol. 1, 529 pp., AGU, Washington, D. C.
- Sciremammano, F., Jr. (1979), A suggestion for the presentation of correlations and their significance levels, *J. Phys. Oceanogr.*, *9*, 1273–1276.
- Strub, P. T., J. S. Allen, A. Huyer, and R. L. Smith (1987), Large-scale structure of the spring transition in the coastal ocean off western North America, *J. Geophys. Res.*, *92*(C2), 1527–1544.
- Winant, C. D., R. C. Beardsley, and R. E. Davis (1987), Moored wind, temperature, and current observations made during Coastal Ocean Dynamics Experiments 1 and 2 over the northern California continental shelf and upper slope, *J. Geophys. Res.*, *92*(C2), 1569–1604.

P. M. Kosro, College of Oceanic and Atmospheric Sciences, Oregon State University, 104 COAS Administration Building, Corvallis, OR 97331-5503, USA. (kosro@coas.oregonstate.edu)